Supplementary Information

Green-solvent-processed formamidinium-based perovskite solar cells with uniform grain growth and strengthened interfacial contact via nanostructured tin oxide layer

Xueyun Wu,[a] Yiting Zheng,[a] Jianghu Liang,[a] Zhanfei Zhang,[a] Congcong Tian,[a] Zhiang Zhang,[a] Yixuan Hu,[a] Anxin Sun,[a] Chenyang Wang,[a] Jianli Wang,[a] Ying Huang,[a] Zhifu Zhang,[a] Kolan Madhav Reddy*[a] and Chun-Chao Chen*[a]

[a] School of Materials Science and Engineering, Shanghai Jiao Tong University, Shanghai 200240, P.R. China

* Corresponding author.

E-mail addresses: kmreddy@sjtu.edu.cn (K. M. Reddy), c3chen@sjtu.edu.cn (C.-C. Chen)

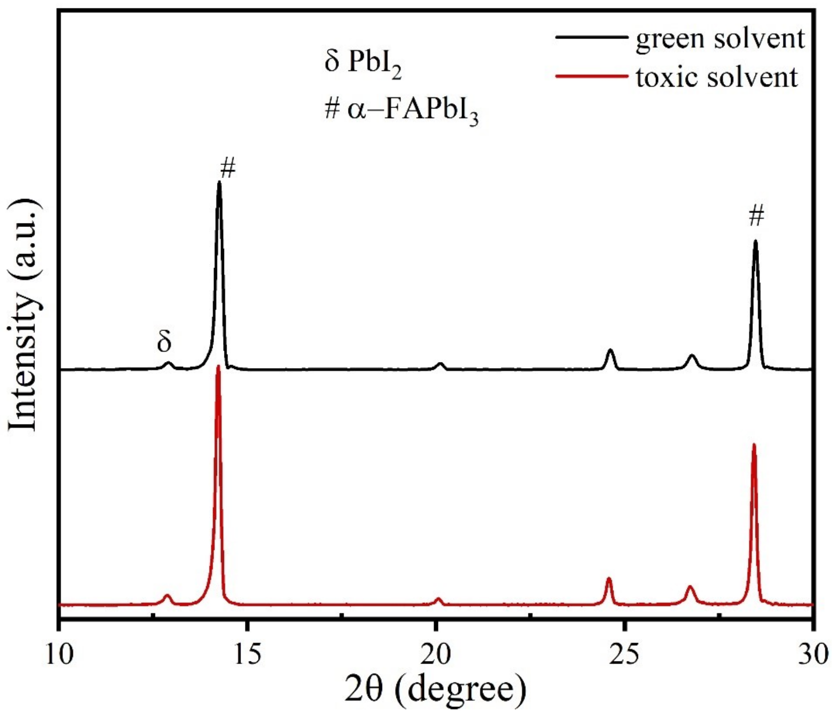

Fig. S1 XRD patterns from top-surfaces of perovskite films prepared via green solvent and toxic solvent, respectively.

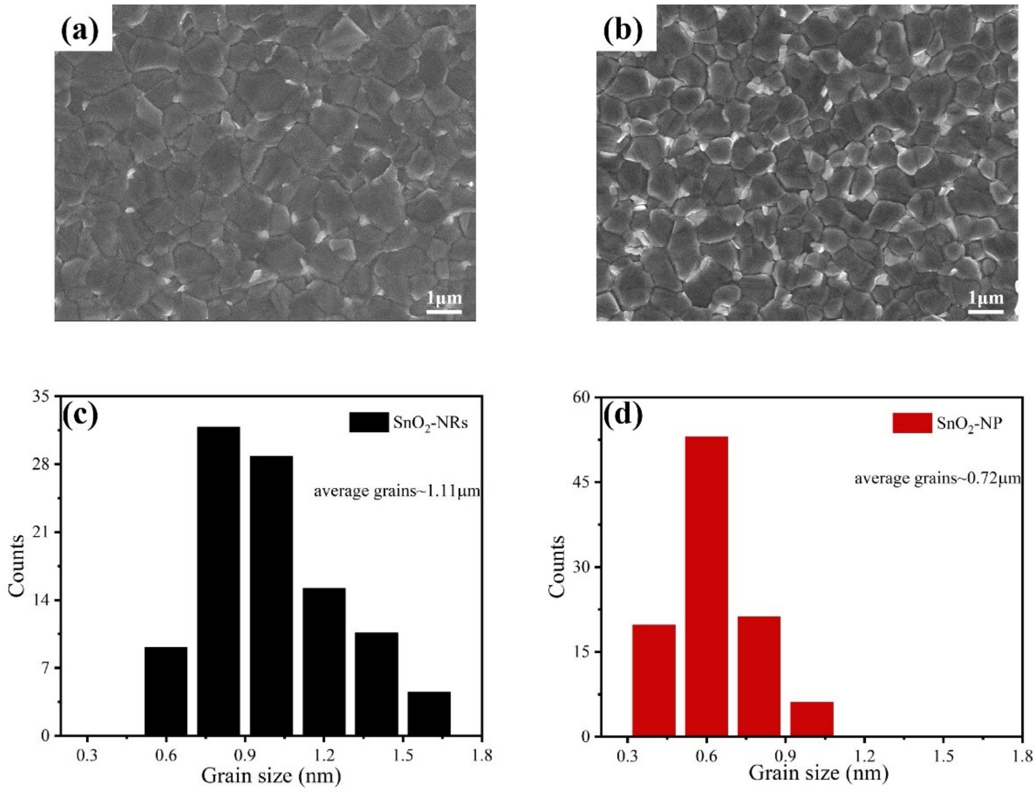

Fig. S2 (a) Top-view SEM image and **(c)** the size distribution of perovskite film based on SnO_2-NRs, respectively. **(b)** Top-view SEM image and **(d)** the size distribution of perovskite film based on SnO_2-NP, respectively.

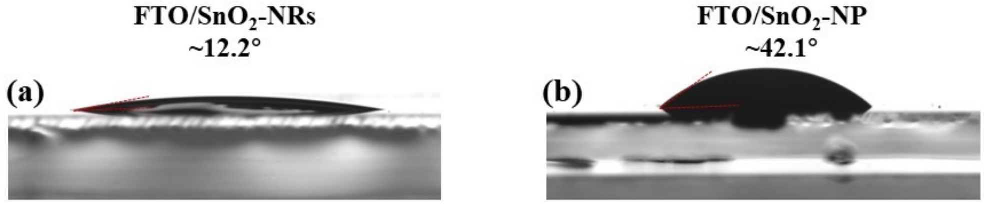

Fig. S3 The deionized water contact angles of **(a)** the SnO_2-NRs and **(b)** SnO_2-NP prepared on FTO substrates.

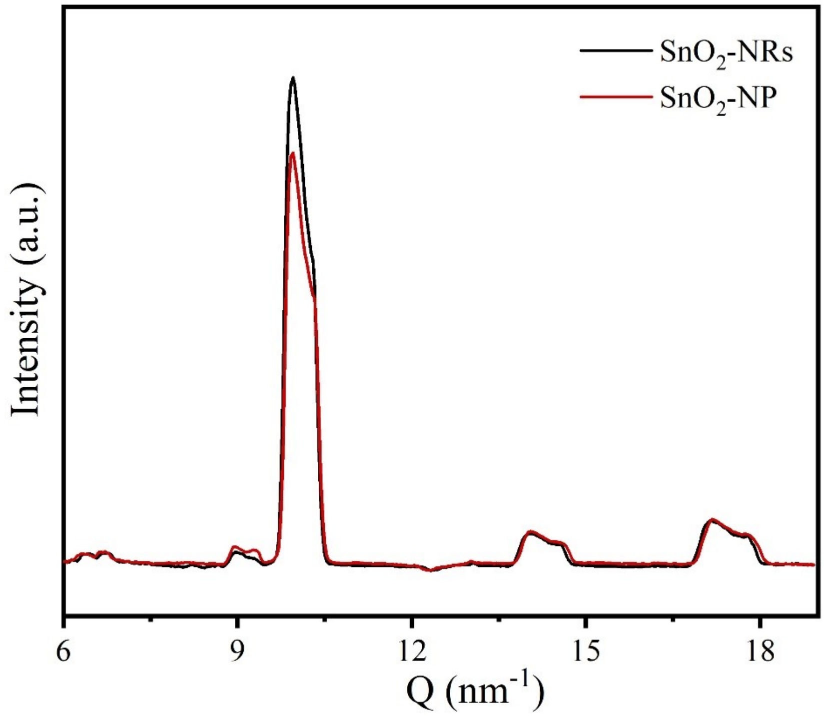

Fig. S4 Integrated intensity profiles along the q_z direction of GIWAXS pattern for SnO_2-NRs and SnO_2-NP substrates.

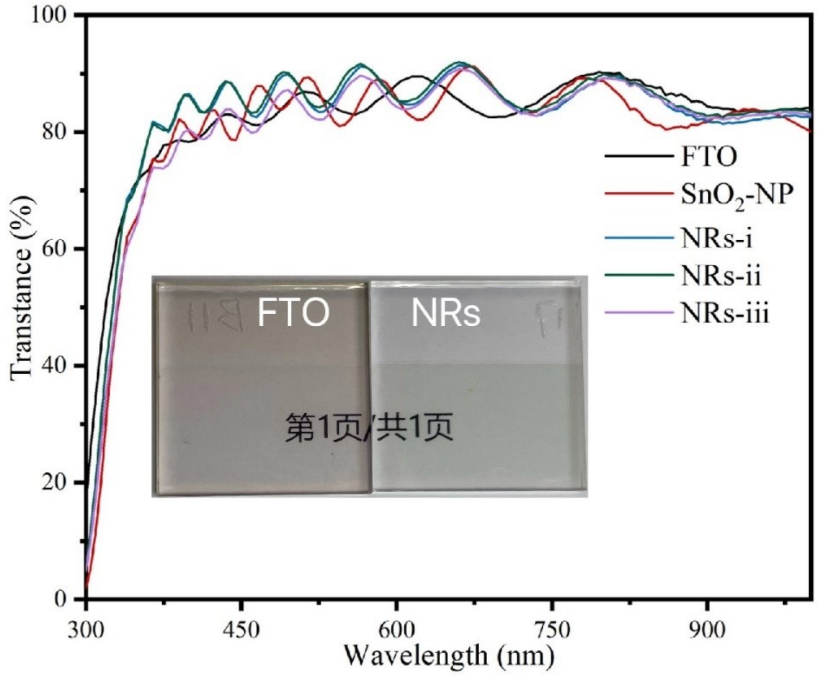

Fig. S5 UV-vis transmittance of bare FTO glass, SnO_2-NP, and SnO_2-NRs in different reaction temperature. The inset shows a typical optical image of the bare FTO glass and FTO/NRs-ii.

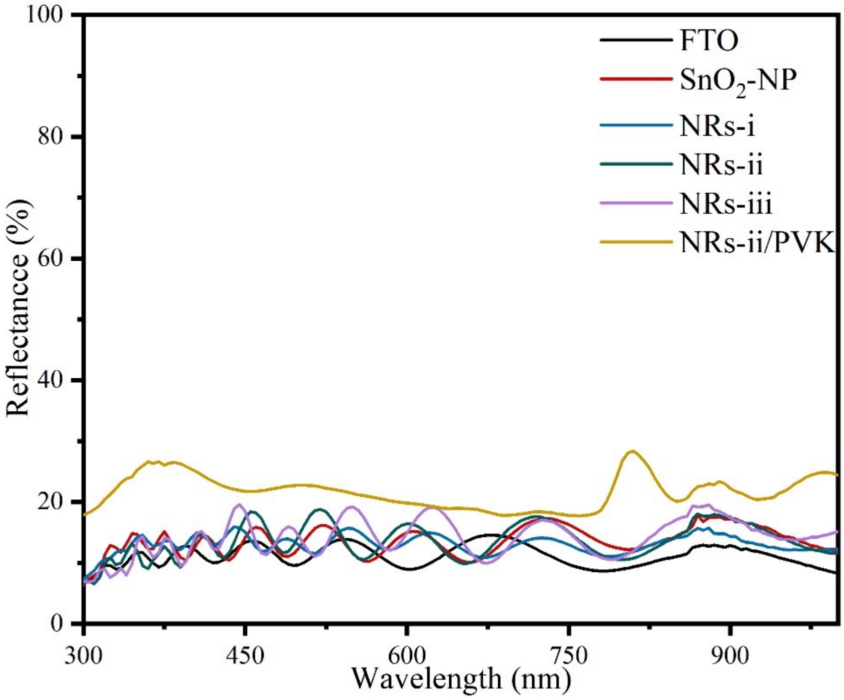

Fig. S6 Diffuse reflectance spectra of different films.

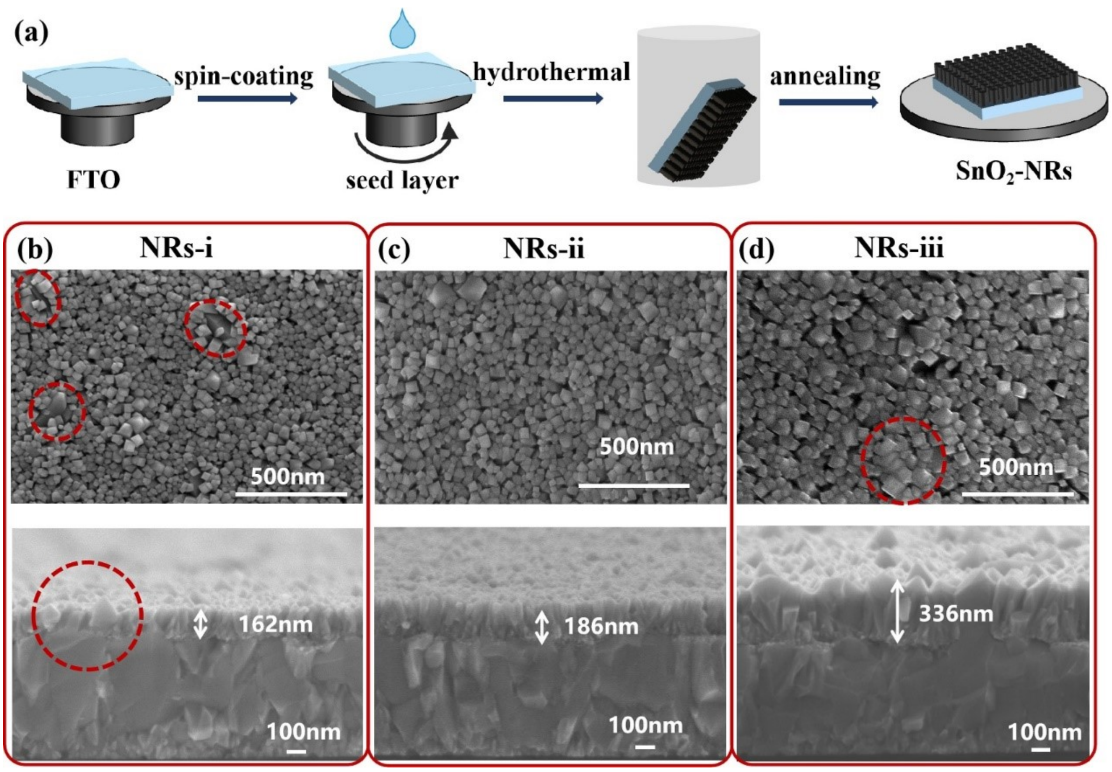

Fig. S7 (a) Schematic of the fabrication procedures of SnO_2-NRs. Top-view and cross-sectional SEM images of SnO_2-NRs in different reaction temperature: **(b)** NRs-i sample at 180℃, **(c)** NRs-ii sample at 200℃, and **(d)** NRs-iii sample at 220℃, respectively.

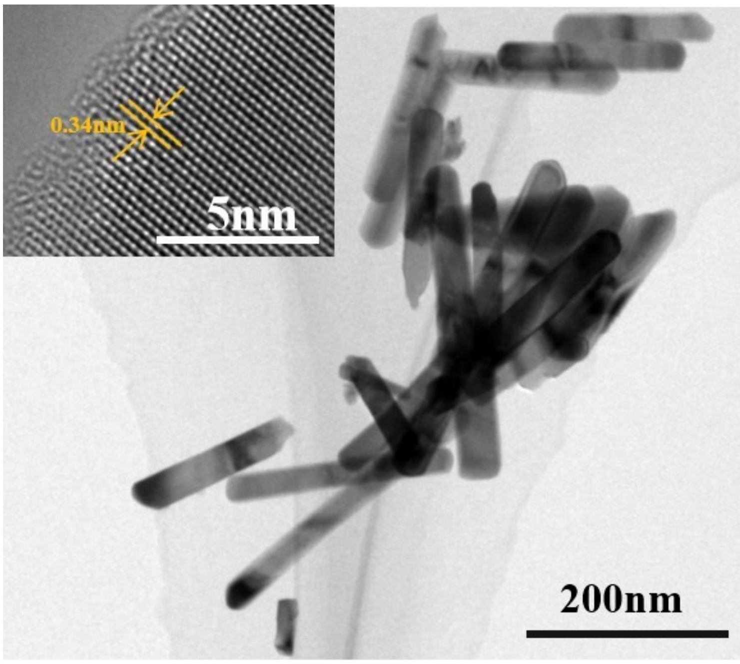

Fig. S8 TEM and HR-TEM images of SnO_2-NRs scraped from NR-ii sample.

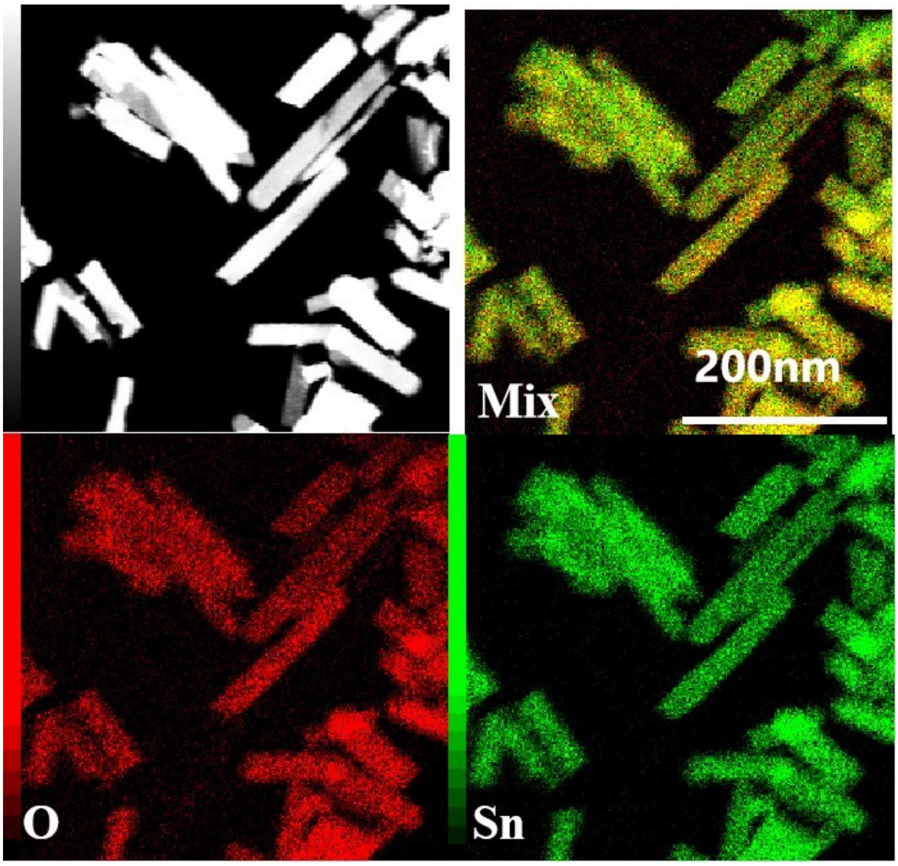

Fig. S9 High-angle annular dark-field (HADDF) STEM image of NRs-ii and energy dispersive X-ray (EDX) elemental mapping images of O, Sn elements.

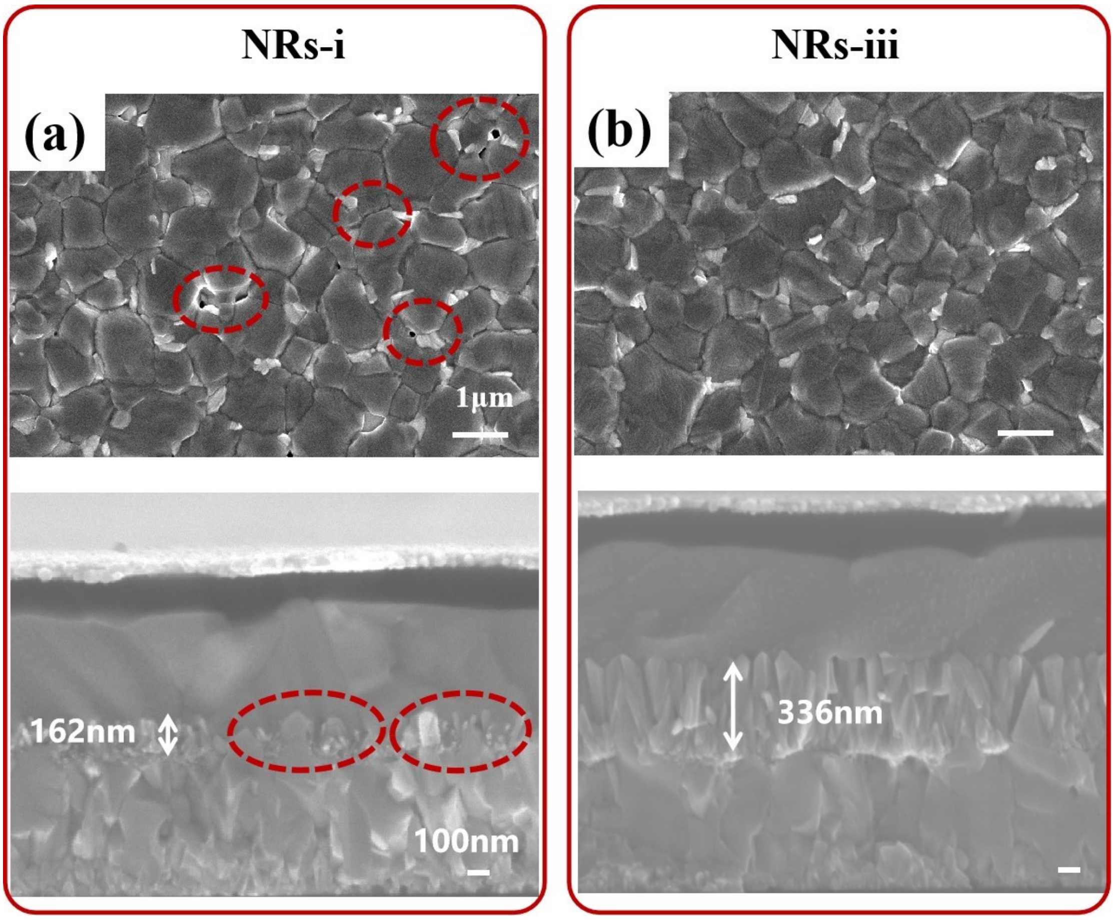

Fig. S10 Top-view and cross-sectional SEM images of perovskite film based on **(a)** NRs-i ETL substrate at 180℃, **(b)** NRs-iii ETL substrate at 220℃

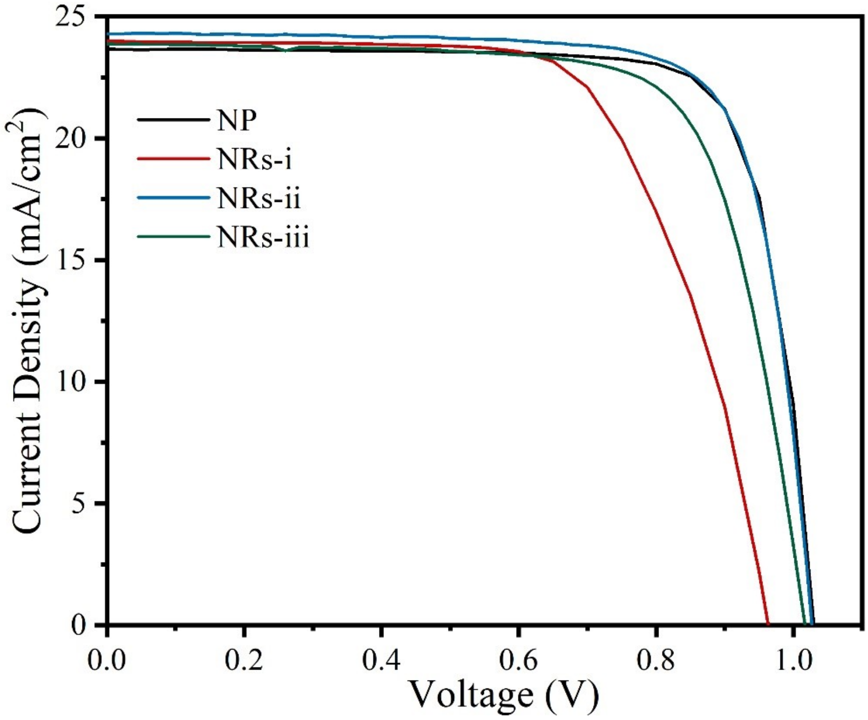

Fig. S11 Current-voltage curves of PSCs based on commercial SnO_2-NP and SnO_2-NRs in different reaction temperature: NRs-i sample at 180°C, NRs-ii sample at 200°C, and NRs-iii sample at 220°C, respectively.

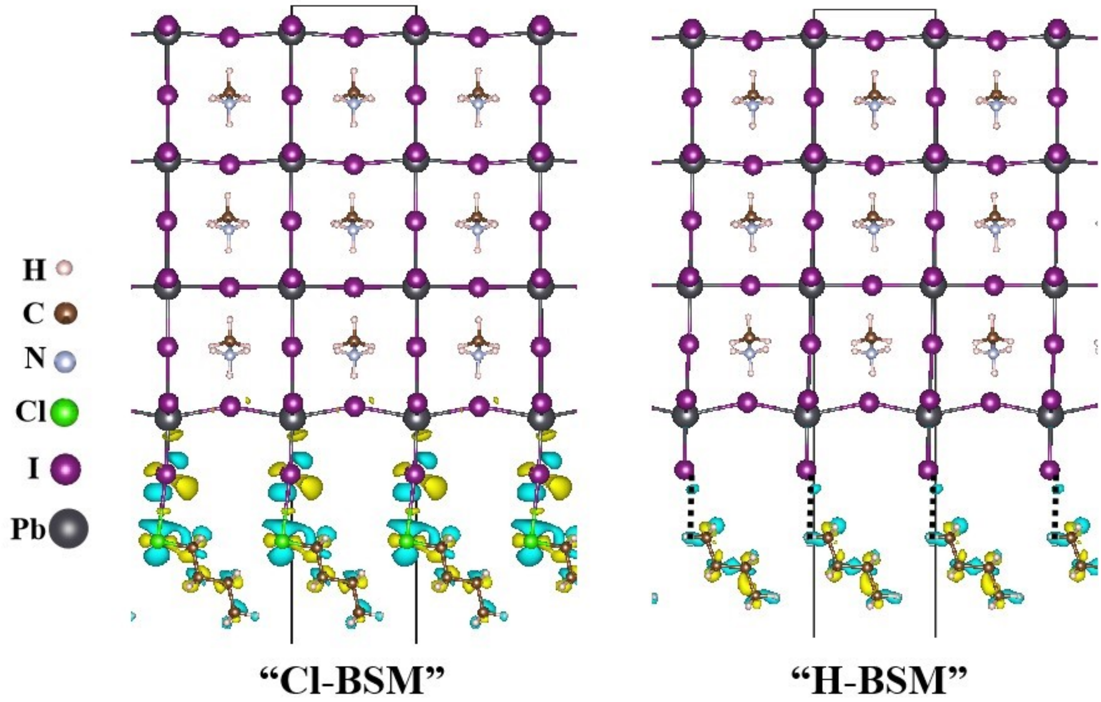

Fig. S12 Charge transfer density difference plots for **(a)** $H(CH_2)_4Cl$ ("Cl-BSM") and **(b)** $H(CH_2)_4H$ ("H-BSM") interfaced with I-terminated $MAPbI_3$ (001) surface. Dashed lines across the interface indicate no bonding.

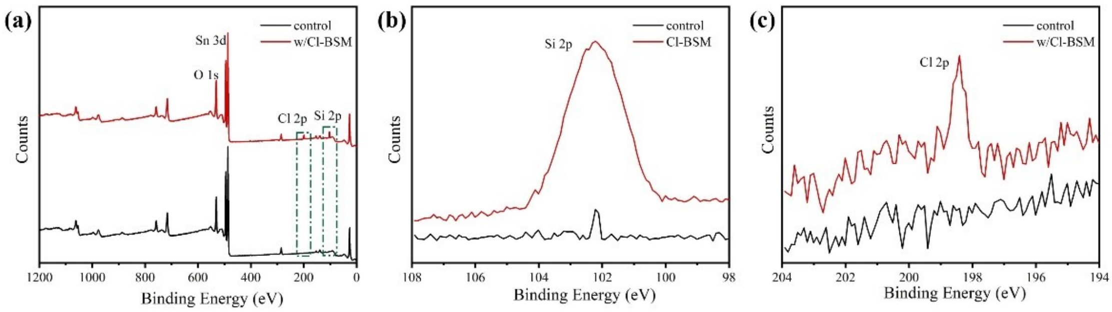

Fig. S13 XPS spectra from top-surface of SnO_2-NRs (control) and Cl-BSM/SnO_2-NRs (w/Cl-BSM): **(a)** typical XPS survey, **(b)** Si 2p core level and **(c)** Cl 2p core level.

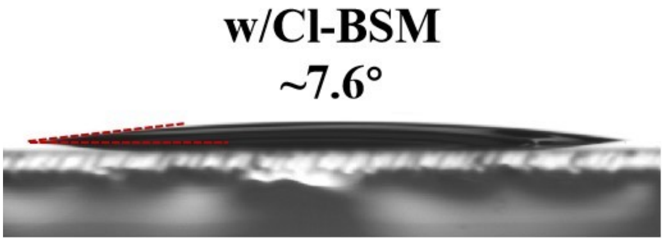

Fig. S14 The deionized water contact angles of SnO_2-NRs/Cl-BSM prepared on FTO substrates.

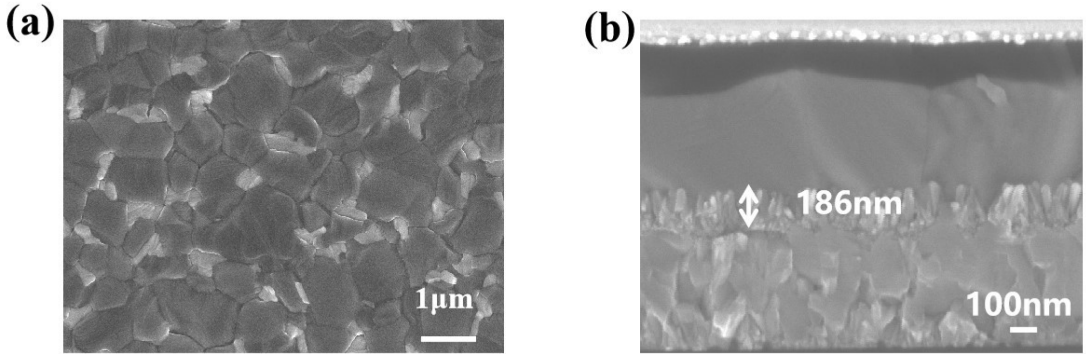

Fig. S15 (a) Top-view SEM image of the perovskite film based on Cl-BSM/SnO_2-NRs and **(b)** cross-sectional SEM image of PSCs device.

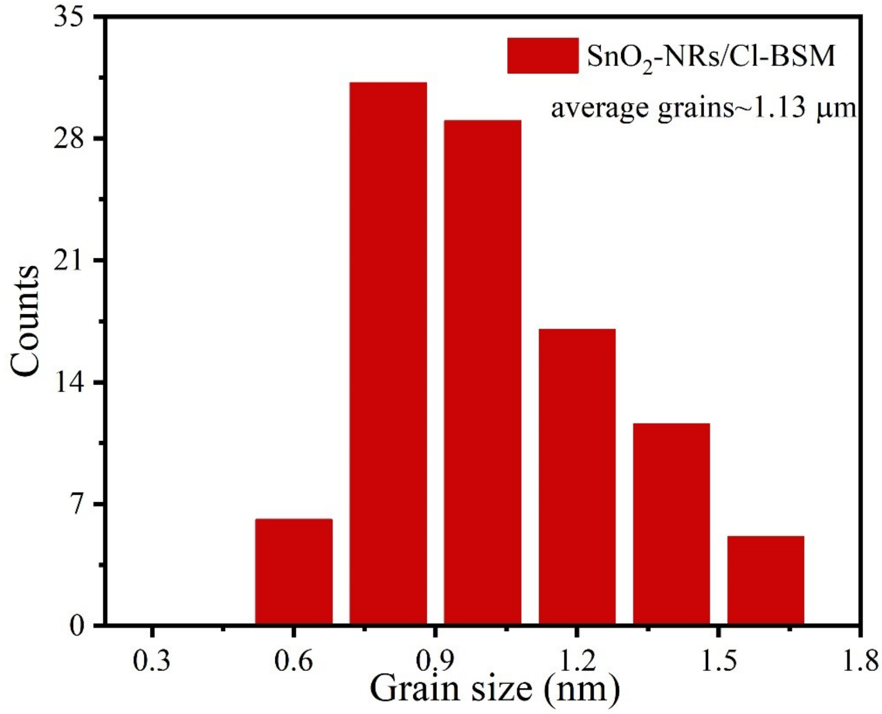

Fig. S16 The size distribution of perovskite film based on SnO_2-NRs/Cl-BSM substrate.

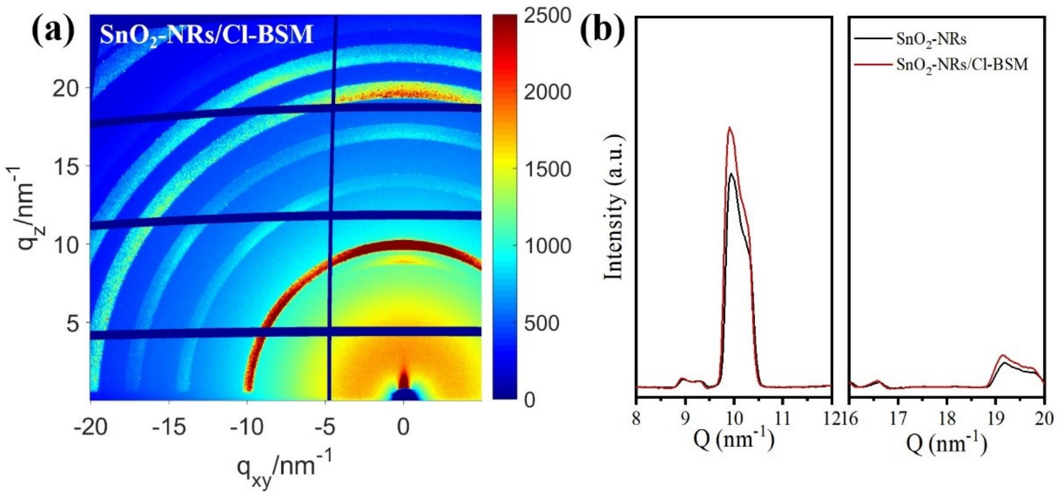

Fig. S17 (a) 2D GIWAXS patterns of perovskite film deposited on SnO_2-NRs/Cl-BSM coated quartz substrates, (b) Integrated intensity profiles along the q_z direction of GIWAXS pattern for SnO_2-NRs and SnO_2-NRs/Cl-BSM substrates.

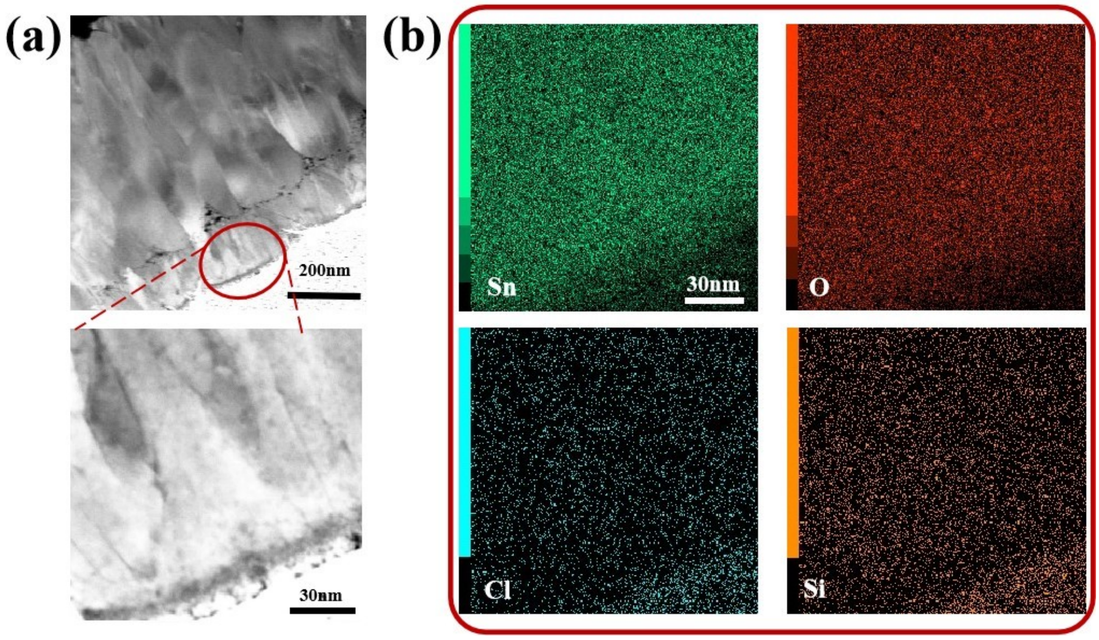

Fig. S18 (a) HAADF-STEM cross-sectional image (top) and zoom-in image of selected area (bottom) of Cl-BSM/SnO_2-NRs grown on FTO substrate. **(b)** EDX cross-sectional elemental mapping images of Sn, Si and Cl elements for Cl-BSM/SnO_2-NRs.

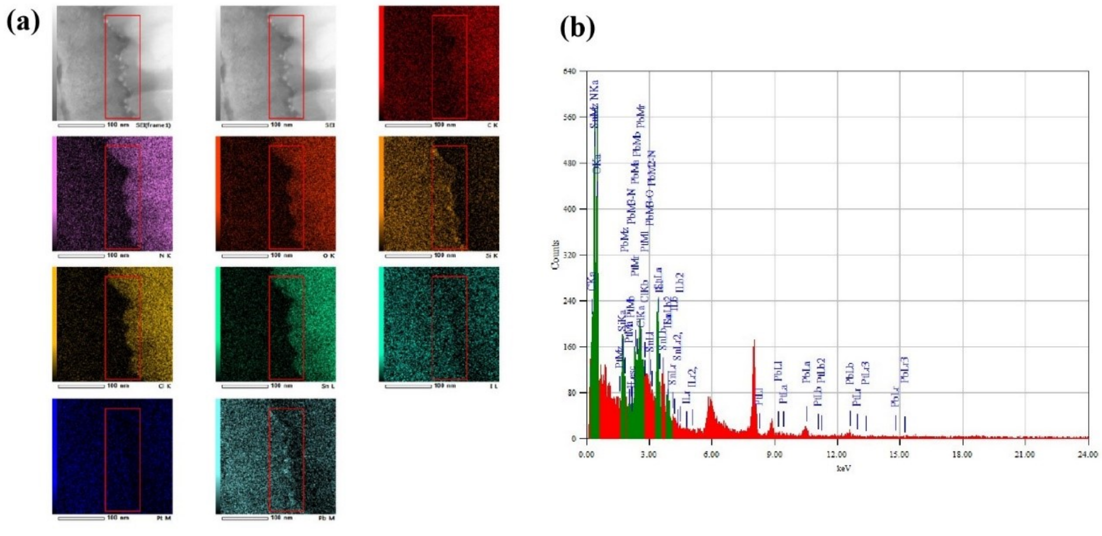

Fig. S19 (a) EDX elemental mapping and **(b)** EDX spectrum of PVK films based on Cl-BSM/SnO_2-NRs.

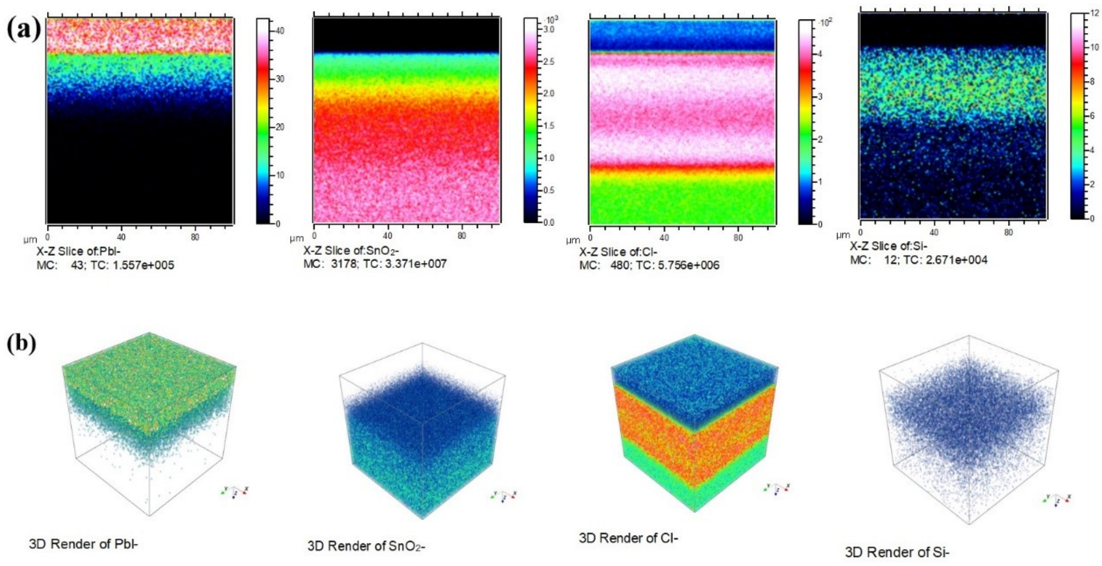

Fig. S20 (a) The X-Z Slice and **(b)** 3D render of various elements SIMS data.

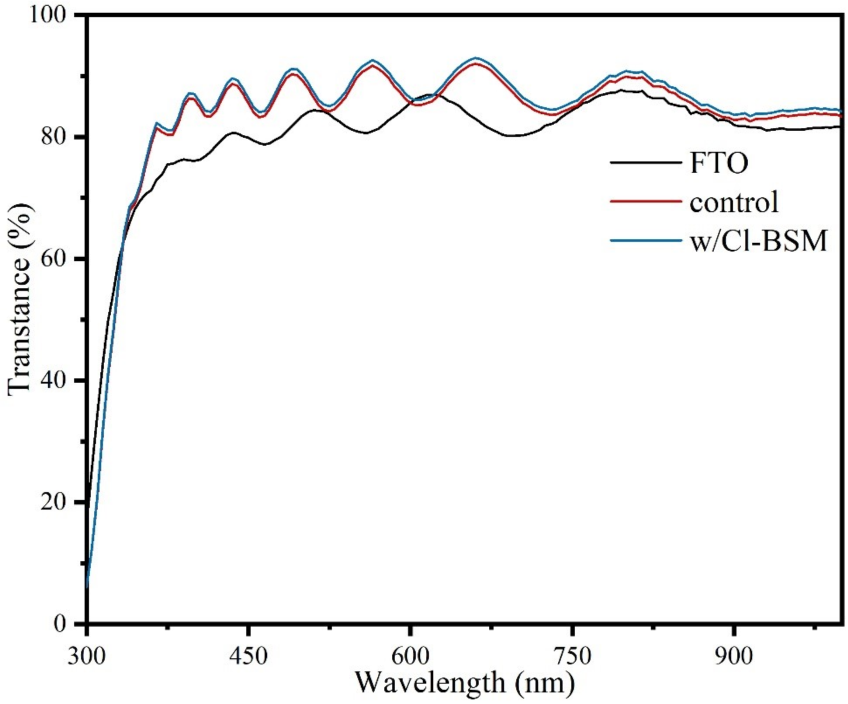

Fig. S21 Transmittance spectra based on bare FTO, SnO_2-NRs, and the Cl-BSM/SnO_2-NRs substrates, respectively.

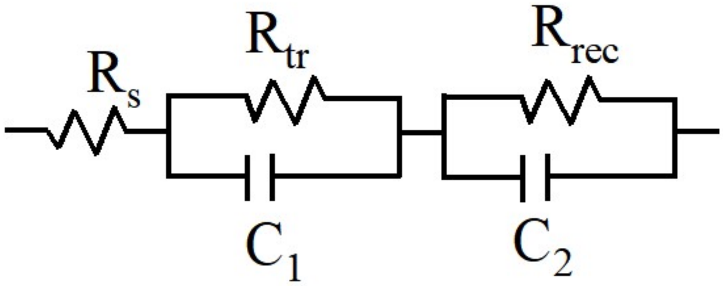

Fig. S22 Equivalent circuit of PSCs based on SnO_2-NRs and SnO_2-NRs/Cl-BSM used for fitting impedance data.

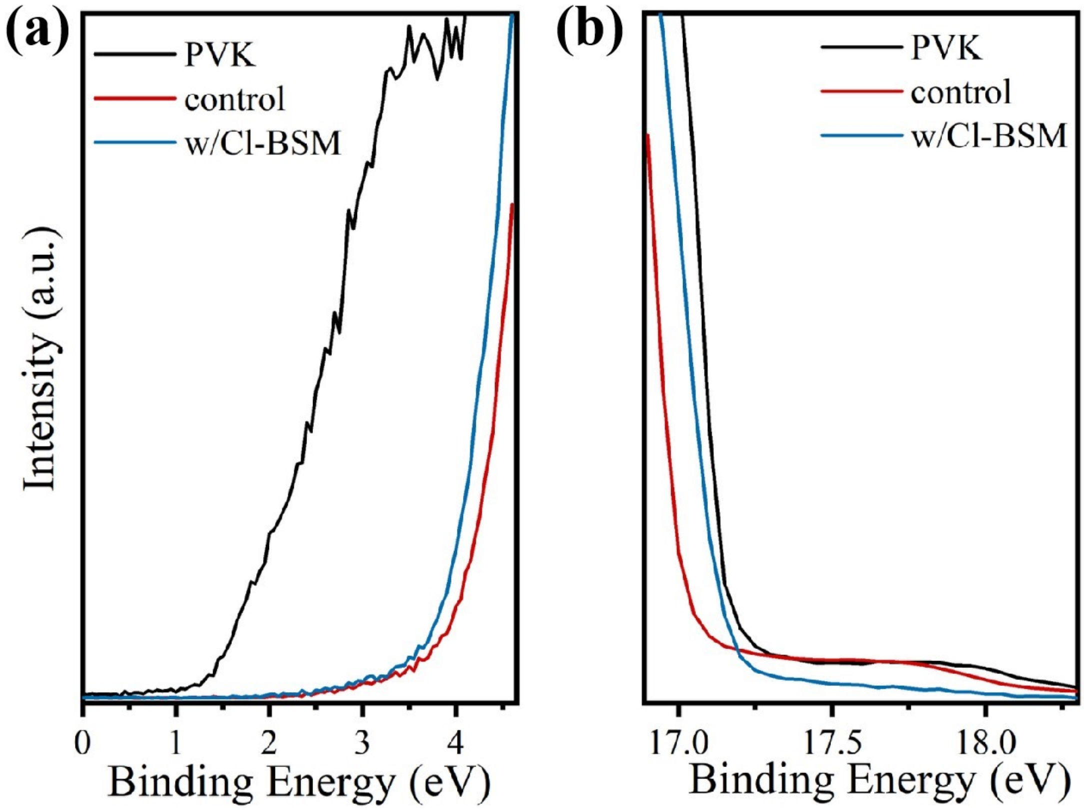

Fig. S23 The UPS spectra on perovskite, SnO_2-NRs and Cl-BSM/SnO_2-NRs films: **(a)** Valance regions (E_{onset}) and **(b)** secondary-electron cutoff (E_{cutoff}). The values of E_{onset} are 1.45 eV, 4.05 eV and 4.03 eV for perovskite, SnO_2-NRs and Cl-BSM/SnO_2-NRs, respectively. The conduction band minimum (E_{CB}) can be calculated from the formular E_{CB} = WF + E_{onset} - E_g, which are 3.99 eV, 4.16 eV and 4.03 eV for perovskite, SnO_2-NRs and Cl-BSM/SnO_2-NRs, respectively.

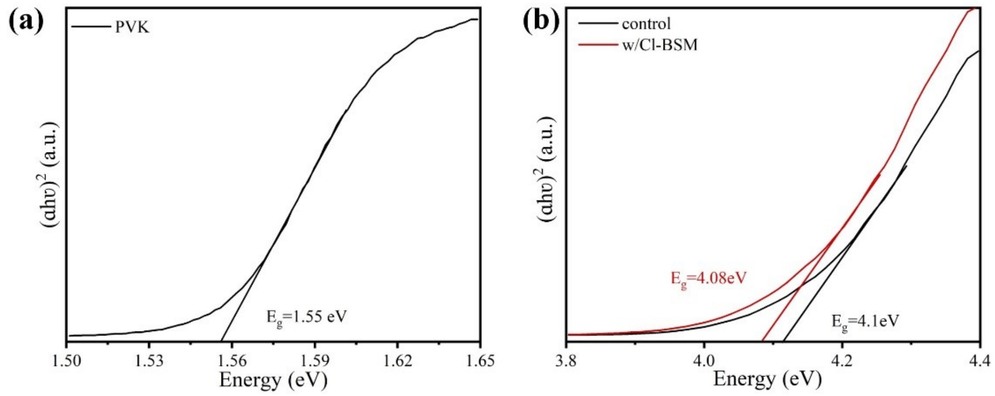

Fig. S24 Tauc plot of **(a)** perovskite and **(b)** SnO_2-NRs and SnO_2-NRs/Cl-BSM films.

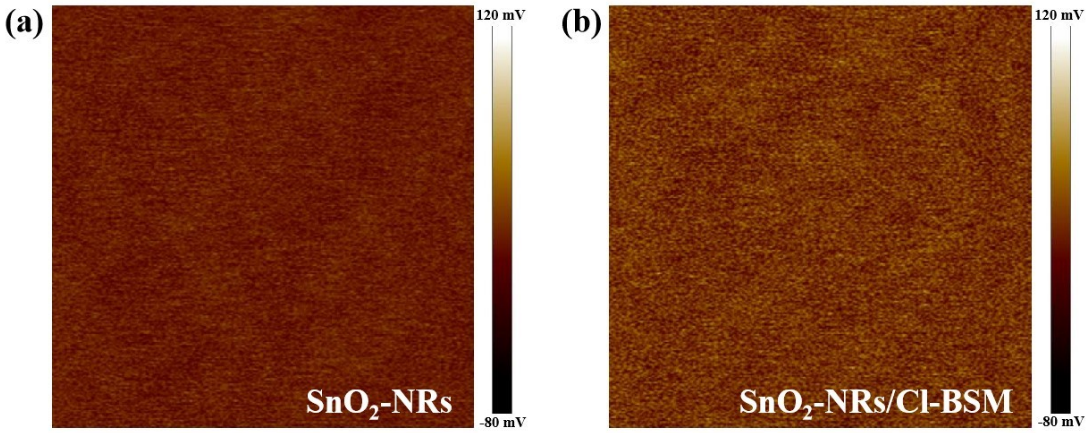

Fig. S25 KPFM images of (a) SnO_2-NRs and (b) SnO_2-NRs/Cl-BSM films.

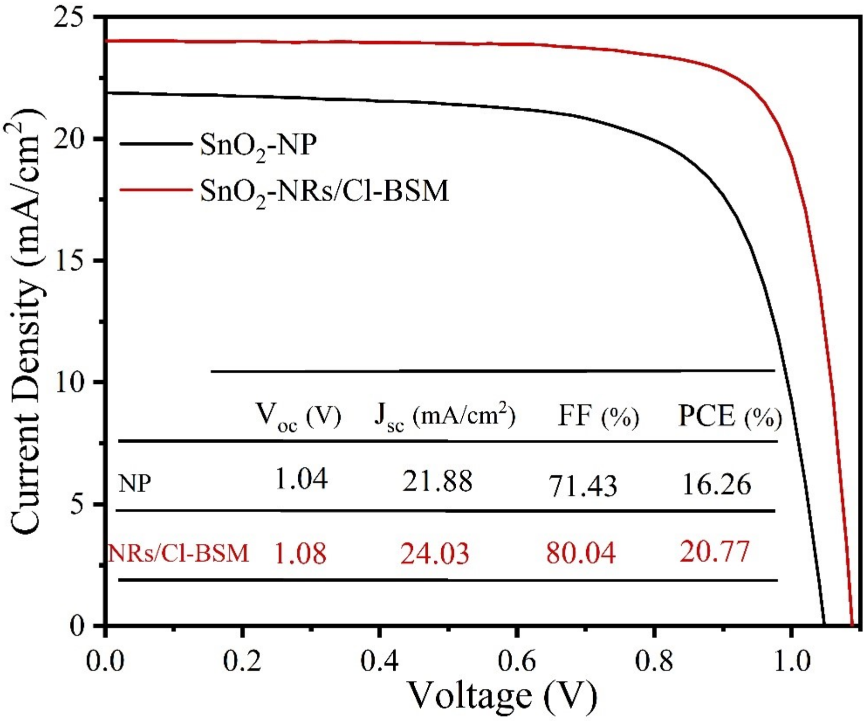

Fig. S26 Current-voltage curves of PSCs based on commercial SnO_2-NP and SnO_2-NRs/Cl-BSM, respectively. Inset shows the relevant paraments of PSCs.

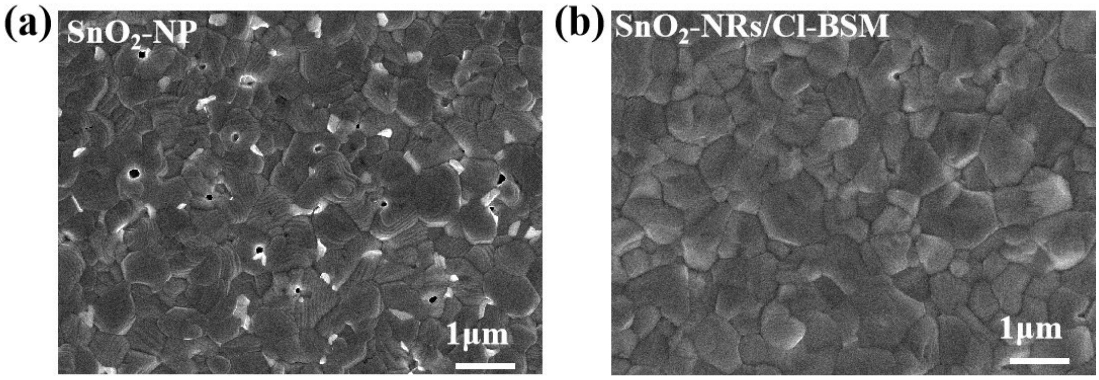

Fig. S27 Top-view SEM images of perovskite film based on SnO_2-NPs and SnO_2-NRs/Cl-BSM, respectively.

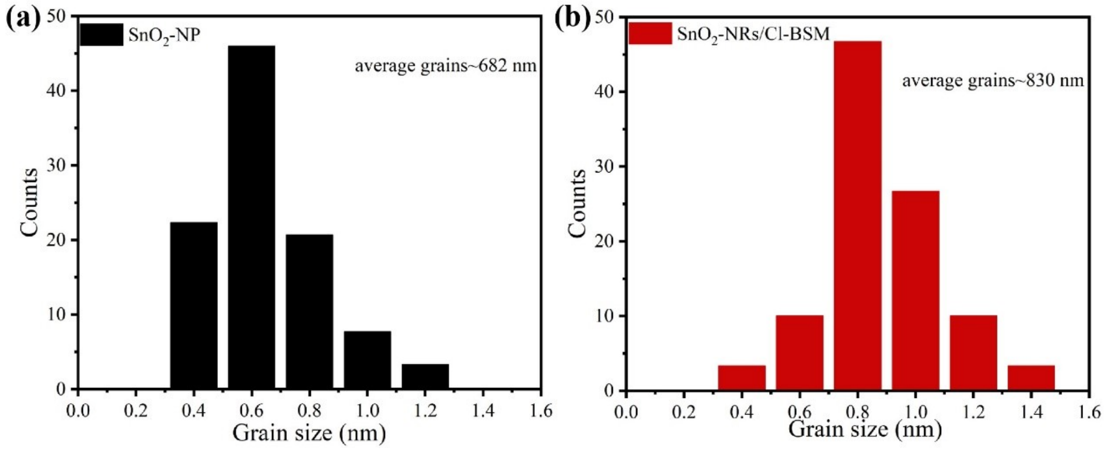

Fig. S28 The size distribution of perovskite film based on SnO_2-NPs and SnO_2-NRs/Cl-BSM, respectively.

Table S1 Performance comparison of recent works about green-solvent engineering

host-solvent	anti-solvent/ air knife	PSCs structure	PCE/ %	year
non-green	**Green**			
DMF/DMSO	diisopropyl ether	FTO/cTiO_2/mTiO_2/Li-TiO_2/perovskite/Spiro/Au	21.26	2022[1]
DMF/DMSO	ethyl acetate /hexane	ITO/SnO_2/perovskite/Spiro/Ag	20.06	2019[2]
DMF/DMSO	anisole	FTO/cTiO_2/mTiO_2/Li-TiO_2/ perovskite/Spiro/Au	20.2	2018[3]
DMF/DMSO	methyl benzoate	FTO/SnO_2/perovskite/Spiro/Au	22.37	2020[4]
DMF/DMSO	tetraethyl orthosilicate	ITO/NiO_x/perovskite/PCBM/BCP/Ag	18.15	2020[5]
DMF/DMSO	methylamine bromide/ethane	ITO/PTAA/perovskite/$PC_{61}BM$/Phen-NADPO/Ag	21.53	2020[6]
DMF/DMPU	air knife	FTO/SnO_2/perovskite/Spiro/Au	20.56	2021[7]
DMF/NMP	antisolvent-free	FTO/SnO_2/perovskite/Spiro/Au	24.02	2022[8]
Green	**Green**			
DMSO	isopropanol	ITO/NiO_x/PTAA/perovskite/$PC_{61}BM$/ BCP/Ag	19.5	2021[9]
DMSO	antisolvent-free	ITO/PTAA /SiO_2-NP/perovskite/PCBM/BCP/Ag	16.7	2021[10]
DMSO/GBL	antisolvent-free	FTO/NiO_x/perovskite/PCBM/PEI/BCP/Ag	17.02	2020[11]
2-Me/ACN	air knife	ITO/PTAA/perovskite/C_{60}/BCP/metal cathode	21.3	2019[12]
2-Me/NMP	antisolvent-free	ITO/MeO-2PACz/perovskite/$PC_{60}BM$/ BCP/Ag	20.39	2022[13]
2-Me/DMSO /MA ethanol	antisolvent-free	FTO/SnO_2/perovskite/Spiro/Au	18.27	2022[14]
TMP/DMF	dibutyl ether	FTO/SnO_2/perovskite/Spiro/Au	20.02	2021[15]
TEP	dibutyl ether	FTO/SnO_2/KCl/perovskite/PEAI/Spiro/Au	20.1	2022[16]
TEP	dibutyl ether	FTO/SnO_2-NRs/Cl-BSM/perovskite/Spiro/Ag	22.42	This work
2-Me	antisolvent-free	FTO/SnO_2-NRs/Cl-BSM/perovskite/Spiro/Ag	20.77	This work

Table S2. Photovoltaic parameters of the PSCs based on commercial SnO_2-NP and SnO_2-NRs in different reaction temperature: NRs-i sample at 180℃, NRs-ii sample at 200℃, and NRs-iii sample at 220℃, respectively.

ETL substrates	J_{sc} (mA/cm^2)	V_{oc} (V)	FF (%)	PCE (%)
SnO_2-NP	23.66	1.00	81.04	19.17
NRs-i	24.01	0.96	67.82	15.63
NRs-ii	**24.30**	1.02	77.86	**19.30**
NRs-iii	23.87	1.02	74.31	18.09

Table S3. DFT results for E_{int} for "BSM" on different surface terminations of $MAPbI_3$ (010). Here, "——" indicates bond formation with charge transfer, and "---" indicates no chemical bond formation

"BSM"/Termination per cell	Cl-SMB/MAI-	H-SMB/MAI-	Cl-SMB/PbI_2-	H-SMB/PbI_2-
E_{int}/eV	-0.176944	-0.147035	-0.465694	-0.226885
Bond Type (Length, Å)	Cl—I (3.42567)	H---I (3.44440)	Cl—Pb (3.19359)	H--- Pb (3.18806)

Table S4. PL decay lifetimes of PVK films on SnO_2-NRs (control) and SnO_2-NRs/Cl-BSM (w/Cl-BSM) coated FTO substrates.

Substrate	τ_1 (ns)	A_1	τ_2(ns)	A_2	τ_t(ns)
Control	1.063	6588.92	78.103	543.47	67.19
w/Cl-BSM	1.797	1171.92	39.714	694.61	37.02

Table S5. The detailed photovoltaic parameters of the champion devices with or without Cl-BSM measured in reverse scan and forward scan at a scan rate of 100 mV/s under simulated AM 1.5G one sun illumination of 100mW/cm^2

Device	Scan direction	J_{sc} (mA/cm^2)	J_{sc} from EQE	V_{oc} (V)	FF (%)	PCE (%)	h (%)
control	reverse scan	24.3	23.3	1.02	77.86	19.3	23.4
	forward scan	24.17		0.92	70.31	15.64	
w/Cl-BSM	reverse scan	**24.6**	**24.2**	**1.12**	**81.36**	**22.42**	**2.6**
	forward scan	24.3		1.12	80.24	21.84	

References

[1] L. Wang, X. Wang, L.-L. Deng, S. Leng, X. Guo, C.-H. Tan, W. C. H. Choy, C.-C. Chen, *Materials Horizons,* 2020, **7**, 934-42.

[2] H. B. Lee, M. K. Jeon, N. Kumar, B. Tyagi, J. W. Kang, *Advanced Functional Materials,* 2019, **29**, 1903213.

[3] M. Yavari, M. Mazloum-Ardakani, S. Gholipour, M. M. Tavakoli, S.-H. Turren-Cruz, N. Taghavinia, M. Grätzel, A. Hagfeldt, M. Saliba, *Advanced Energy Materials,* 2018, **8**, 1800177.

[4] Y. Yun, F. Wang, H. Huang, Y. Fang, S. Liu, W. Huang, Z. Cheng, Y. Liu, Y. Cao, M. Gao, L. Zhu, L. Wang, T. Qin, W. Huang, *Adv Mater,* 2020, **32**, e1907123.

[5] M. Wang, Q. Fu, L. Yan, J. Huang, Q. Ma, M. Humayun, W. Pi, X. Chen, Z. Zheng, W. Luo, *Chemical Engineering Journal,* 2020, **387**, 123966.

[6] W. Xu, Y. Gao, W. Ming, F. He, J. Li, X. H. Zhu, F. Kang, J. Li, G. Wei, *Adv Mater,* 2020, **32**, e2003965.

[7] D. Lee, K. Lim, J. Lee, N. Park, *Journal of Materials Chemistry A*, 2021, **9**, 3018-3028.

[8] T. Bu, L. Ono, J. Li, J. Su, G. Tong, W. Zhang, Y. Liu, J. Zhang, J. Chang, S. Kazaoui, F. Huang, Y.-B. Cheng, Y. Qi, *Nature Energy*, 2022, **7**, 528-536.

[9] S. Shan, Y. Li, H. Wu, T. Chen, B. Niu, Y. Zhang, D. Wang, C. Kan, X. Yu, L. Zuo, H. Chen, *SusMat,* 2021, **1**, 537-44.

[10] J. Küffner, J. Hanisch, T. Wahl, J. Zillner, E. Ahlswede, M. Powalla, *ACS Applied Energy Materials,* 2021, **4**, 11700-10.

[11] H. Huang, Y. Tian, C. Huang, F. Li, C. Chu, M. Lee, C. Huang, F. Su, *ACS Appl Mater Interfaces,* 2020, **12**, 26041-9.

[12] Y. Deng, C. Van Brackle, X. Dai, J. Zhao, B. Chen, J. Huang, *Sci Adv*, 2019, **5**, eaax7537.

[13] S. Lee, S. Hong, H. Kim, *ACS Appl Mater Interfaces*, 2022, **14**, 39132-39140.

[14] Q. Zhang, G. Ma, A. Green, K. Gollinger, J. Moore, T. Demeritte, C. Ray, A.

Hill, X. Gu, E. Morgan, M. Feng, S. Banerjee, Q. Dai, *ACS Applied Energy Materials*, 2022, **5**, 1487-1495.

[15] Yun. Y, Vidyasagar. D, Lee. M, Gong. O. Y, Jung. J, Jung. H. S, Kim. D. H, Lee. S, *Adv Sci,* 2021, **8**, e2102492-501.

[16] Cao. X, Hao. L, Liu. Z, Su. G, He. X, Zeng. Q, Wei. J, *Chemical Engineering Journal,* 2022, **437**, 135458-66.